Label-free biosensing with high sensitivity in dual-core microstructured polymer optical fibers

Christos Markos,[1, 4,*] Wu Yuan,[2] Kyriakos Vlachos,[1] Graham E. Town,[3] and Ole Bang[2]

*[1]Department of Computer Engineering and Informatics, University of Patras,
Patra, 26500, Greece*
*[2]DTU Fotonik, Department of Photonics Engineering, Technical University of Denmark,
2800 Kongens Lyngby, Denmark*
*[3]Department of Electronic Engineering, Macquarie University,
NSW 2109, Australia*
*[4]Theoretical and Physical Chemistry Institute, National Hellenic Research Foundation,
Athens, 11635, Greece*
[*]cmarkos@ceid.upatras.gr

Abstract: We present experimentally feasible designs of a dual-core microstructured polymer optical fiber (mPOF), which can act as a highly sensitive, label-free, and selective biosensor. An immobilized antigen sensing layer on the walls of the holes in the mPOF provides the ability to selectively capture antibody biomolecules. The change of the layer thickness of biomolecules can then be detected as a change in the coupling length between the two cores. We compare mPOF structures with 1, 2, and 3 air-holes between the solid cores and show that the sensitivity increases with increasing distance between the cores. Numerical calculations indicate a record sensitivity up to 20 nm/nm (defined as the shift in the resonance wavelength per nm biolayer) at visible wavelengths, where the mPOF has low loss.

©2011 Optical Society of America

OCIS codes: (130.5460) Polymer waveguides; (060.2370) Fiber optics sensors; (060.4005) Microstructured fibers; (280.1415) Biological sensing and sensors.

References and links

1. J. C. Knight, T. A. Birks, P. St. J. Russell, and D. M. Atkin, "All-silica single-mode optical fiber with photonic crystal cladding," Opt. Lett. **21**(19), 1547–1549 (1996).
2. M. A. van Eijkelenborg, M. Large, A. Argyros, J. Zagari, S. Manos, N. Issa, I. Bassett, S. Fleming, R. McPhedran, C. M. de Sterke, and N. A. Nicorovici, "Microstructured polymer optical fibre," Opt. Express **9**(7), 319–327 (2001).
3. G. Emiliyanov, J. B. Jensen, O. Bang, P. E. Hoiby, L. H. Pedersen, E. M. Kjær, and L. Lindvold, "Localized biosensing with Topas microstructured polymer optical fiber," Opt. Lett. **32**(5), 460–462 (2007).
4. G. Emiliyanov, J. B. Jensen, O. Bang, P. E. Hoiby, L. H. Pedersen, E. M. Kjær, and L. Lindvold, "Localized biosensing with Topas microstructured polymer optical fiber: erratum," Opt. Lett. **32**(9), 1059–1059 (2007).
5. K. Nielsen, H. K. Rasmussen, A. J. L. Adam, P. C. M. Planken, O. Bang, and P. U. Jepsen, "Bendable, low-loss Topas fibers for the terahertz frequency range," Opt. Express **17**(10), 8592–8601 (2009).
6. T. M. Monro, D. J. Richardson, and P. J. Bennet, "Developing holey fibers for evanescent field devices," Electron. Lett. **35**(14), 1188–1189 (1999).
7. J. B. Jensen, L. H. Pedersen, P. E. Hoiby, L. B. Nielsen, T. P. Hansen, J. R. Folkenberg, J. Riishede, D. Noordegraaf, K. Nielsen, A. Carlsen, and A. Bjarklev, "Photonic crystal fiber based evanescent-wave sensor for detection of biomolecules in aqueous solutions," Opt. Lett. **29**(17), 1974–1976 (2004).
8. L. Rindorf, P. E. Høiby, J. B. Jensen, L. H. Pedersen, O. Bang, and O. Geschke, "Towards biochips using microstructured optical fiber sensors," Anal. Bioanal. Chem. **385**(8), 1370–1375 (2006).
9. M. E. Bosch, A. J. R. Sánchez, F. S. Rojas, and C. B. Ojeda, "Recent development in optical fiber biosensors," Sensors **7**(6), 797–859 (2007).
10. X. Fan, I. M. White, S. I. Shopova, H. Zhu, J. D. Suter, and Y. Sun, "Sensitive optical biosensors for unlabeled targets: A review," Anal. Chim. Acta **620**(1-2), 8–26 (2008).
11. A. Hassani, and M. Skorobogatiy, "Design of the microstructured optical fiber-based surface plasmon resonance sensors with enhanced microfluidics," Opt. Express **14**(24), 11616–11621 (2006).
12. A. Wang, A. Docherty, B. T. Kuhlmey, F. M. Cox, and M. C. J. Large, "Side-hole fiber sensor based on surface plasmon resonance," Opt. Lett. **34**(24), 3890–3892 (2009).
13. L. Rindorf, and O. Bang, "Highly sensitive refractometer with a photonic-crystal-fiber long-period grating," Opt. Lett. **33**(6), 563–565 (2008).

14. J. M. Fini, "Microstructure fibers for optical sensing in gases and liquids," Meas. Sci. Technol. **15**(6), 1120–1128 (2004).
15. Y. Zhang, H. Shibru, K. L. Cooper, and A. Wang, "Miniature fiber-optic multicavity Fabry-Perot interferometric biosensor," Opt. Lett. **30**(9), 1021–1023 (2005).
16. L. Rindorf, J. B. Jensen, M. Dufva, L. H. Pedersen, P. E. Høiby, and O. Bang, "Photonic crystal fiber long-period gratings for biochemical sensing," Opt. Express **14**(18), 8224–8231 (2006).
17. J. R. Ott, M. Heuck, C. Agger, P. D. Rasmussen, and O. Bang, "Label-free and selective nonlinear fiber-optical biosensing," Opt. Express **16**(25), 20834–20847 (2008).
18. D. K. C. Wu, B. T. Kuhlmey, and B. J. Eggleton, "Ultrasensitive photonic crystal fiber refractive index sensor," Opt. Lett. **34**(3), 322–324 (2009).
19. B. T. Kuhlmey, S. Coen, and S. Mahmoodian, "Coated photonic bandgap fibres for low-index sensing applications: cutoff analysis," Opt. Express **17**(18), 16306–16321 (2009).
20. W. Yuan, G. E. Town, and O. Bang, "Refractive Index Sensing in an All-Solid Twin-Core Photonic Bandgap Fiber," IEEE Sens. J. **10**(7), 1767–1770 (2010).
21. G. E. Town, W. Yuan, R. McCosker, and O. Bang, "Microstructured optical fiber refractive index sensor," Opt. Lett. **35**(6), 856–858 (2010).
22. B. Sun, M. Y. Chen, Y. K. Zhang, J. C. Yang, J. Q. Yao, and H. X. Cui, "Microstructured-core photonic-crystal fiber for ultra-sensitive refractive index sensing," Opt. Express **19**(5), 4091–4100 (2011).
23. Y. Gao, N. Guo, B. Gauvreau, M. Rajabian, O. Skorobogata, E. Pone, O. Zabeida, L. Martinu, C. Dubois, and M. Skorobogatiy, "Consecutive solvent evaporation and co-rolling techniques for polymer multilayer hollow fiber preform fabrication," J. Mater. Res. **21**(9), 2246–2254 (2006).
24. J. B. Jensen, P. E. Hoiby, G. Emiliyanov, O. Bang, L. Pedersen, and A. Bjarklev, "Selective detection of antibodies in microstructured polymer optical fibers," Opt. Express **13**(15), 5883–5889 (2005).
25. B. J. Mangan, J. C. Knight, T. A. Birks, P. St. J. Russell, and A. H. Greenaway, "Experimental study of dual core photonic crystal fibre," Electron. Lett. **36**(16), 1358–1359 (2000).
26. W. E. P. Padden, M. A. van Eijkelenborg, A. Argyros, and N. A. Issa, "Coupling in a twin-core microstructured polymer optical fiber," Appl. Phys. Lett. **84**(10), 1689–1691 (2004).
27. M. Hansen, and G. E. Town, "All-optical switching in dual-core microstructured optical fibres modeled using beam-propagation", *Proceedings, 28th Australian Conference on Optical Fibre Technology (ACOFT 2003), Melbourne*
28. M. Hansen, and G. E. Town, "Properties of dual-core couplers in microstructured optical fibres," *Proceeedings, 28th European Conference on Optical Communications (ECOC/IOOC 2003)*, Vol. 3, p.616–617, Rimini, September, 2003.
29. M. Large, L. Poladian, G. Barton, and M. A. van Eijkelenborg, *Microstructured Polymer Optical Fibres*, (Springer, 2008), Chap. 7.
30. K. Nielsen, H. K. Rasmussen, P. U. Jepsen, and O. Bang, "Broadband terahertz fiber directional coupler," Opt. Lett. **35**(17), 2879–2881 (2010).
31. G. E. Town, R. F. Copperwhite, R. Kribich, K. O'Dwyer, and B. D. MacCraith, "Comparison of multimode and multichannel couplers for evanescent sensing of refractive index,*"* in *Proc. 30th Australian Conf. Optical Fiber Technol.*, Sydney, Australia, 2005.
32. B. T. Kuhlmey, B. J. Eggleton, and D. K. C. Wu, "Fluid-Filled Solid-Core Photonic Bandgap Fibers," J. Lightwave Technol. **27**(11), 1617–1630 (2009).
33. K. Nielsen, D. Noordegraaf, T. Sorensen, A. Bjarklev, and T. Hansen, "Selective filling of photonic crystal fibres," J. Opt. A, Pure Appl. Opt. **7**(8), L13–L20 (2005).
34. E. Palik, *Handbook of Optical Constants of Solids I–III* (Academic, 1998).
35. I. D. Nikolov, and C. D. Ivanov, "Optical Plastic Refractive Measurements in the Visible and the Near-Infrared Regions," Appl. Opt. **39**(13), 2067–2070 (2000).
36. Z. Zhu, and T. Brown, "Full-vectorial finite-difference analysis of microstructured optical fibers," Opt. Express **10**(17), 853–864 (2002).
37. J.-J. Gau, E. H. Lan, B. Dunn, C.-M. Ho, and J. C. S. Woo, "A MEMS based amperometric detector for E. coli bacteria using self-assembled monolayers," Biosens. Bioelectron. **16**(9-12), 745–755 (2001).
38. J. Laegsgaard, O. Bang, and A. Bjarklev, "Photonic crystal fiber design for broadband directional coupling," Opt. Lett. **29**(21), 2473–2475 (2004).

1. Introduction

Microstructured optical fibers (MOFs) based on either silica [1], or polymers, such as poly(methyl methacrylate) (PMMA) [2] or topas [3–5], are a class of fibers in which the cladding has an array of holes running along the entire length of the fiber. MOF-based platforms are interesting for biosensing applications, because biological samples can be probed by the guided light inside the holes without removing the coating and cladding of the fiber, maintaining thus the robustness of the sensor [6–10]. In addition, the air holes of the MOF may hold a biological sample volume of a few nL per cm of the fiber while still achieving high sensitivity, which is a significant advantage for biosensing applications. Geometrical manipulation of the fiber cross-section gives MOFs an extreme ability to

increase the interaction of the guided light with the sample by a number of different configurations and working principles that have already been demonstrated. Typical label-free, fiber-optic biosensors are based on tracking the shift in a resonance (surface plasmon, gratings, Fabry-Pérot, etc.) introduced by the presence of a biological agent [11–22].

Given that a pre-required ability for a label-free biosensor to function is that it is able to work as a sensitive refractive index sensor we will discuss biosensors and refractive index sensors in parallel. The best sensitivities of label-free MOF biosensors to date have been reported in devices in which the sample modifies the phase matching between coupled modes. Rindorf *et al.* demonstrated experimentally a sensitivity of 1.4 nm/nm, i.e. a 1.4 nm shift in resonance wavelength per nm biolayer of a long-period grating [16], and recently Ott *et al.* predicted a sensitivity of 10.4 nm/nm in a four-wave mixing based label-free biosensor [17]. In terms of refractive index sensing, Wu *et al.* recently demonstrated a sensitivity of 30,100 nm per refractive index unit (nm/RIU) in a refractive index guiding dual-core silica MOF operating above cut-off of a selectively filled analyte channel [18]. This device, however, was not suitable for sensing refractive indices less than that of the fiber host. It has now been shown that coating the holes and using fluorinated polymer MOFs will allow to extend the regime of operation to low indices, such as water [19]. Yuan *et al.* demonstrated the design of an all-solid dual-core photonic bandgap fiber, in which a single hole between the cores acts as microfluidic channel for the analyte [20]. The predicted sensitivity was 70,000 nm/RIU. Town *et al.* reported a dual-core MOF sensor that could also use simple single-wavelength intensity-based sensing with a sensitivity (change in transmittance per refractive index unit) that could be increased to 169,711%/RIU by selectively filling the two holes between the cores of the coupler [21]. More recently, Sun et al. proposed a refractive index sensor based on a microstructured-core MOF, where coupling changes between the conventional and the microstructured-core depend on the analyte filled into the holes of the core [22]. The authors in [22] demonstrated sensitivity up to 8500 nm/RI, while the detection limit was 2.02x10-6 for an analyte with refractive index of 1.33.

The experimental record sensitivity of 1.4 nm/nm was obtained using a long-period grating and requires therefore post-processing of the fiber, as does any grating or surface-plasmon based sensor. The theoretically predicted record sensitivity of 10.4 nm/nm [17] uses the inherent nonlinearity of the fiber material for four-wave mixing and thus requires no post-processing. However, it requires a long length of the fiber and high power. The dual-core MOFs have not yet been investigated for label-free biosensing but only for refractive index sensing. The dual-core MOF based refractive index sensors reported so far either require selective filling [18,19,21,22], have very small holes [21], or have an all-solid bandgap structure that requires to find two suitable materials that are also compatible for drawing [20], which can be very difficult [23].

In this work, we have numerically investigated a dual-core mPOF biosensor made of PMMA, in which an antigen sensor layer can selectively capture a thin layer of around 5 nm of antibody biomolecules via the antigen-antibody binding process [7, 24]. Dual-core MOFs were first fabricated in silica by Mangan *et al.* [25] and in polymer by Padden *et al.* [26], with some of the early modeling work being done by Hansen and Town [27, 28]. The main advantage of considering polymer MOFs and PMMA is that biomolecules can be attached directly to the surface of the holes of the fiber [24], avoiding in this way any further functionalization; combined with the fact that mPOFs can now be routinely fabricated with a wealth of different structures [29]. In other polymers, such as topas, intermediate layers still have to be used to immobilize the capture layer [3, 4]. So even though topas mPOF couplers are possible [30], we will focus on PMMA here.

The increment of the layer thickness due to the immobilization of antibody biomolecules will directly affect the coupling coefficient of the dual-core mPOF coupler, and thereby change the transmittance of the coupler. We have compared three dual-core mPOF biosensor structures with different separation distance between the two cores (1, 2 and 3 holes separation). Apriori, the largest separation should result in the largest sensitivity [31] and this is what has been observed. A sensitivity of around 20 nm/nm is achieved for a 15 cm long

device at visible wavelengths, where the mPOF exhibits the lowest loss. This is the highest reported sensitivity for a MOF biosensor. The structural parameters of the mPOF biosensor are kept experimentally feasible, both in terms of the pitch and hole diameter of the preform as well as in terms of the device length, when taking into consideration the loss and ease of fabrication and handling.

2. Design parameters of mPOF biosensor

The proposed dual-core mPOF is a standard index guiding fiber with a hexagonal hole structure with pitch $\Lambda = 2$ μm and hole size d = 1 μm, as shown in Fig. 1(a). The relative hole size of d/Λ = 0.5 assures single-mode operation of the sensor with water in the holes. We consider structures, in which the two cores are separated by either 1, 2, or 3 holes, i.e., by either 2Λ, 3Λ or 4Λ. We consider a maximum separation distance between the cores of 3 holes (or 4Λ) mainly because when the distance between the cores increases, small fluctuations in fiber diameter due to fabrication tolerances may affect the performance of the sensor. In this section, we first focus on the 3Λ (or 2-hole) separation for the detailed operation, while in the next sections we compare the different separations in terms of sensitivity. We consider as an example label-free antibody detection using the highly selective antigen-antibody binding [24]. The mPOF biosensor is functionalized for antibody detection by immobilization of an antigen sensor layer onto the walls of the holes. This sensor layer can consist of a functionalization layer of a certain thickness (e.g., biotin) in addition to the antigen layer. We will as an example consider a sensor suitable for sensing the antibody α-streptavidin with thickness $t_a = 5$ nm [37]. In this case the antigen layer has a thickness of about 10 nm [37]. In order to be able to make a direct comparison of our biosensor with the record sensitivity of the four-wave mixing biosensor proposed in [17], we consider a thickness of the sensor layer of $t_s = 40$ nm, as illustrated in Fig. 1(c). We consider PMMA as the fiber material because it allows easy binding of biomolecules [24]. It is worth noting that in a PMMA mPOF, the thickness of the sensor layer can be reduced to 10 nm (the thickness of the antigen layer only) compared to a silica MOF, since intermediate functionalization layers can be avoided. We calculated the sensitivity for both a thickness of $t_s = 40$ nm and $t_s = 10$ nm and we found the difference to be small (section 3.2, Fig. 6-a). In this section, we focus on the case of $t_s = 40$ nm.

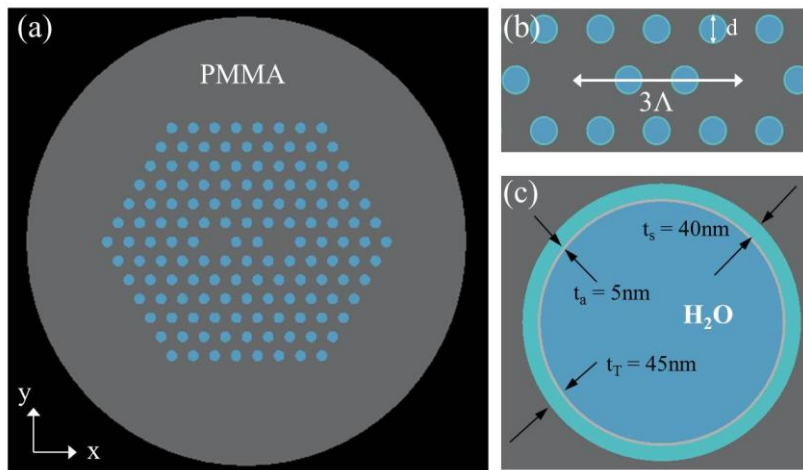Fig. 1. (a) Hexagonal hole pattern of a dual-core mPOF biosensor with pitch $\Lambda = 2$ μm and hole diameter d = 1 μm. (b) The two cores are separated by a distance of 3Λ. (c) Water filled hole with a sensor layer of $t_s = 40$ nm and an attached layer of biomolecules of thickness $t_a = 5$ nm.

We always consider the holes of the mPOF biosensor filled with water, mainly for two reasons: 1) because water reduces the refractive index contrast between cladding-core,

enabling thus single-mode operation of the fiber above 500 nm, and 2) the introduction of samples in aqueous solution into the sensor might leave remnants of water, which from an experimental point of view is difficult to remove. Infiltration techniques have been previously demonstrated both theoretically and experimentally, where water infusion can be achieved either applying capillary forces or with low pressure in pressure chambers, even in holes with diameters of 1 micron [32, 33]. The dispersion of water and PMMA has been included in our calculations based on their Sellmeier equations [34, 35]. The refractive index and material dispersion of the layer of biomolecules depend on the orientation of the molecules. However, experimental measurements with MOF biosensors have shown that a refractive index of n = 1.45 for α-streptavidin biomolecules is a realistic assumption [16]. We therefore use n = 1.45 and neglect dispersion of the thin layer of biomolecules. The numerical investigation of the dual-core mPOF biosensor is done by employing the fully vectorial integrated mode solver of the commercially available *Lumerical FDTD solutions* software. The effective indices of the fundamental guided modes are computed based on finite difference analysis using Yee's mesh and the index averaging technique [36].

The proposed structures of the dual-core mPOF biosensor can be fabricated with a two-stage drawing process using a realistic preform of diameter of 6 cm with holes of 2 mm diameter drilled into it. An important parameter of the proposed PMMA-based biosensor is the loss. We have experimentally measured the loss of a single-core PMMA mPOF with a diameter of 130 μm fabricated at DTU Fotonik with the same relative hole size of $d/\Lambda = 0.5$ as the proposed dual-core structure (see inset in Fig. 2).

We used the cut-back technique and measured the output power of the mPOF at 14 different lengths, starting from 55 cm, using a broadband source (SuperK from NKT photonics). The measurements are performed with great care in order to minimize errors from coupling in/out instabilities, cleaving quality, bending effects, etc. Figure 2 shows the experimentally measured loss of the fiber to be around 5 - 30 dB/m which is significantly higher than the record of 0.1 - 1 dB/m for the range of 500 - 850 nm stated in [29]. However, the mPOF is made from a cheap low-purity PMMA with non-optimal preform fabrication conditions. Further optimization in terms of cooling liquid used in preform drilling and proper washing and drying in clean atmosphere after drilling, are underway. Given the loss we will use fiber lengths less than 15 cm.
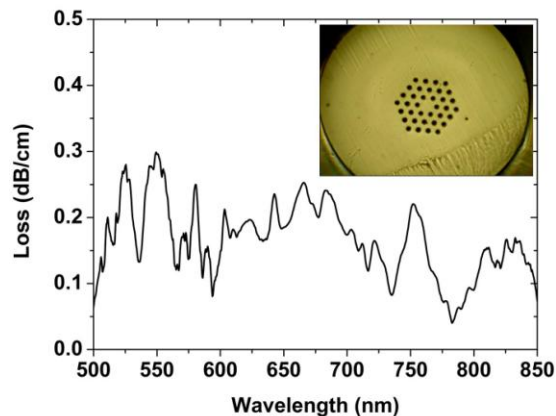

Fig. 2. Loss profile of an mPOF with $d/\Lambda = 0.5$. Inset: Cross-section of the fiber.

3. Results and discussion

3.1 Sensing mechanism – transmittance

The cores of the mPOF form a balanced linear directional coupler, in which light in the two cores interact due to a weak overlap of their evanescent fields, enabling a periodic transfer of the optical power from one core to the other [27,28,38]. This coupling can be understood and

analyzed in terms of a pair of supermodes; a symmetric (even) and an asymmetric (odd) supermode. Figures 3(a-b) shows the even and odd x-polarized intensity distribution of the supermodes of a water-filled dual-core mPOF with 2 holes between the solid cores, while Fig. 3(c) shows the effective index difference between the x- and y-polarization of the supermodes. Although the difference between the effective indices is relative small, the two orthogonal polarizations may yield differences in the coupling length. In any case, the sensing mechanism remains the same and thus only one (x-polarization) is shown here. Experimentally, the elimination of the other polarization can be done via the insertion of a polarizer as proposed by Wu *et al*. [18].
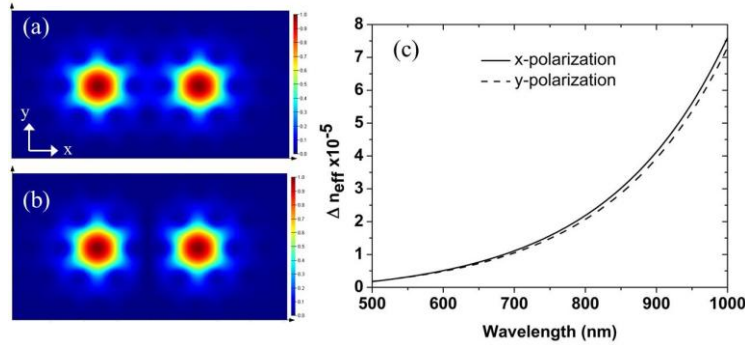

Fig. 3. Electric field distribution of the even (a) and odd (b) x-polarized supermode at 1 μm wavelength for the mPOF structure with 3Λ separation between the cores. (c) Effective index difference of the x (solid line) and y (dotted line) polarizations.

Given the effective index difference, we can now determine how the capture of a biolayer of a certain thickness t on the walls of the holes of the mPOF affects the coupling length of the biosensor, L_C, which is given by:

$$L_C = \frac{\lambda}{2\Delta n_{eff}(\lambda, t)} \qquad (1)$$

The coupling length of the dual-core mPOF with 2 holes between the cores decreases monotonically with wavelength as shown in Fig. 4(a). Addition of the antigen sensor layer with 40 nm thickness onto the walls of the holes in the mPOF significantly reduces the coupling length, for all wavelengths. The additional 5 nm thick layer of captured α-streptavidin biomolecules decreases the coupling length even further.
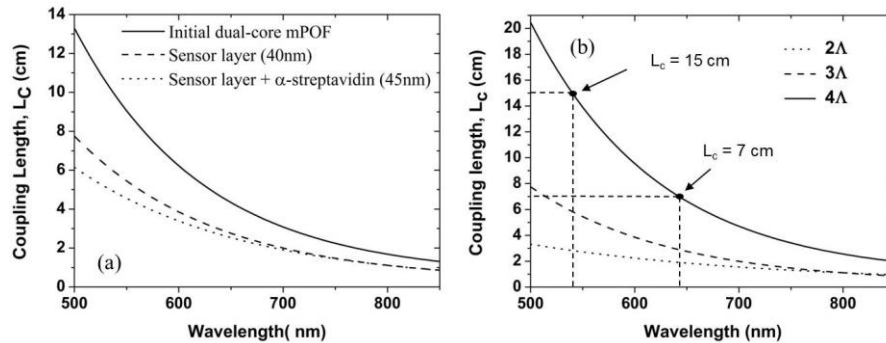

Fig. 4. (a) Coupling length versus wavelength of the dual-core mPOF biosensor with two holes (3Λ) between the cores, and a 0 nm (solid line), 40nm (dashed), and 45 nm biolayer immobilized onto the walls of the holes. (b) Coupling length of the dual-core mPOF with immobilized 40 nm sensor layer for 2Λ (dotted), 3Λ (dashed), and 4Λ (solid) separation distance between the cores.

In Fig. 4(b) we compare the coupling length for a dual-core biosensor (i.e., a coupler with 40 nm sensor layer) with 1, 2, and 3 holes between the cores. As expected we see that the coupling length increases with the core-separation because the overlap of the evanescent tails of the core modes becomes weaker. We also see that 3 holes is the maximum separation we can use if we want a fiber length of less than 15 cm below 650 nm.

From the coupling length L_C, we can calculate the transmittance of the biosensor using the following expression:

$$T = \cos^2(\frac{\pi L/2}{L_C}) \tag{2}$$

where L is the length of the fiber. Figure 5 shows the transmittance (output power P_{OUT} relative to input power P_{IN}) of a 7 cm long dual-core biosensor in the spectral range 500-800 nm. It clearly demonstrates how the addition of a biolayer changes the transmission by blue-shifting the extrema. Such a transmission spectrum allows for two different sensing schemes: (1) In the perhaps simplest scheme one can use a single-wavelength source and sense the transmitted power, in which case the highest sensitivity would be obtained by biasing the sensor to 50% transmittance [20,21]. (2) One can also use a broadband source and detector and sense the change in wavelength of an extremum [20].
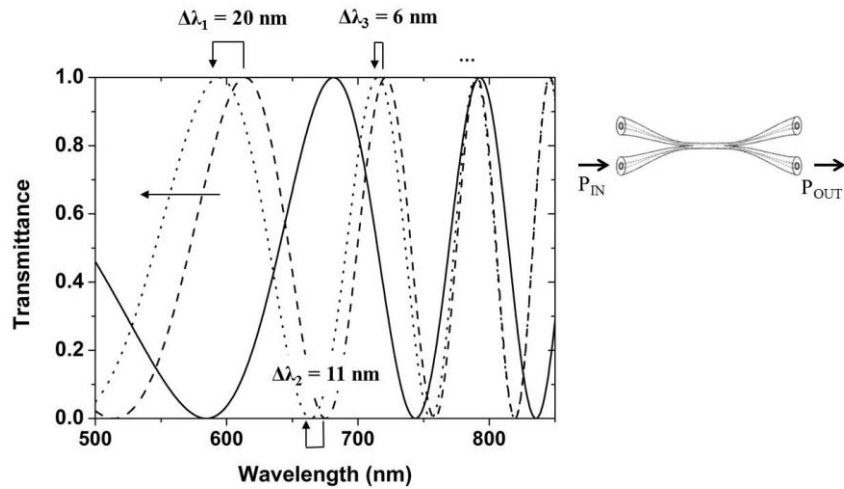

Fig. 5. Plot of transmittance Pout/Pin of a 7 cm long dual-core mPOF biosensor versus wavelength (solid line), with an immobilized 40 nm antigen layer (dashed), and with a captured antibody layer of an additional 5 nm thickness (dotted). Separation distance between the cores is 2Λ. (Right) Simple schematic of the coupler with definition of Pout and Pin.

Here we focus on the broadband scheme and track the shift of the extrema, as one would when using a long-period grating [16] or four-wave mixing for the sensing [17]. From Fig. 5 we see that the shift is largest for the lowest wavelength extrema. The first extremum will always be a minimum, which is obtained for $L_C = L$, for which T = 0. However, from Fig. 4 we see that L_C is always below 7 cm in the 500-800 nm window for a 45 nm biolayer. Thus the capture of the 5nm antibody biolayer should shift this minimum out of the window, which is confirmed in Fig. 5. The first maximum at $\lambda_1 = 605$ nm blue-shifts by 20 nm when the 5 nm antibody biolayer is captured, which gives a sensitivity of 4 nm/nm. The longer wavelength extrema shift less, e.g., the second minimum at $\lambda_2 = 670$ nm shifts only $\Delta\lambda_2 = 11$ nm.

In the next section we will detail how the sensitivity depends on the core separation and fiber length and show that we can obtain a record sensitivity of 20 nm/nm by increasing the separation to 3 holes.

3.2 Sensitivity

Here we calculate and compare the sensitivities obtained for 1, 2, and 3 hole separation between the cores of the dual-core mPOF, based on the simple principle of tracking the resonant wavelength shift of transmittance as a function of the biolayer thickness, using the methodology described in the previous section. Because the coupling length increases significantly when going to a 3 hole separation, we will consider both a 7 cm coupler and a 15 cm coupler. We will consider only a wavelength window of 500-900 nm, so if a capture of biomolecules blue-shifts a given resonance outside the window, then this point is not included in the sensitivity curve.

The sensitivity can be expressed as $S = \Delta\lambda/\Delta t$ (nm/nm), where Δt is the change of the biolayer thickness when the antibody biomolecules are captured, which in our case is 5 nm. We have so far used an antigen sensor layer of thickness 40 nm in order to compare directly the sensitivity of our biosensor with the previous record of 10.4 nm/nm [17]. However, the proposed dual-core mPOF biosensor exhibits similar sensitivity also for a sensor layer of thickness 10 nm, as confirmed in Fig. 6(a) for the case with one hole in between the two cores (blue triangles). In both cases Fig. 6(a) shows that the sensitivity is between 1.5 and 1.4 nm/nm at around 550 nm, while decreasing monotonically as the wavelength increases. We have considered a device length of both 7 cm (black squares) and 15 cm (red dots). The sensitivity for the two device lengths will lie on the same curve $S(\lambda)$, but by going to a longer length one can move further down in wavelength on the $L_C(\lambda)$ curve in Fig. 4 and thereby obtain a higher sensitivity. However, with only one hole separation the sensitivity curve is rather flat and so nothing is gained by using a longer fiber length, when taking into account that the loss is then also larger. Clearly one hole separation is not enough to achieve a good sensitivity.
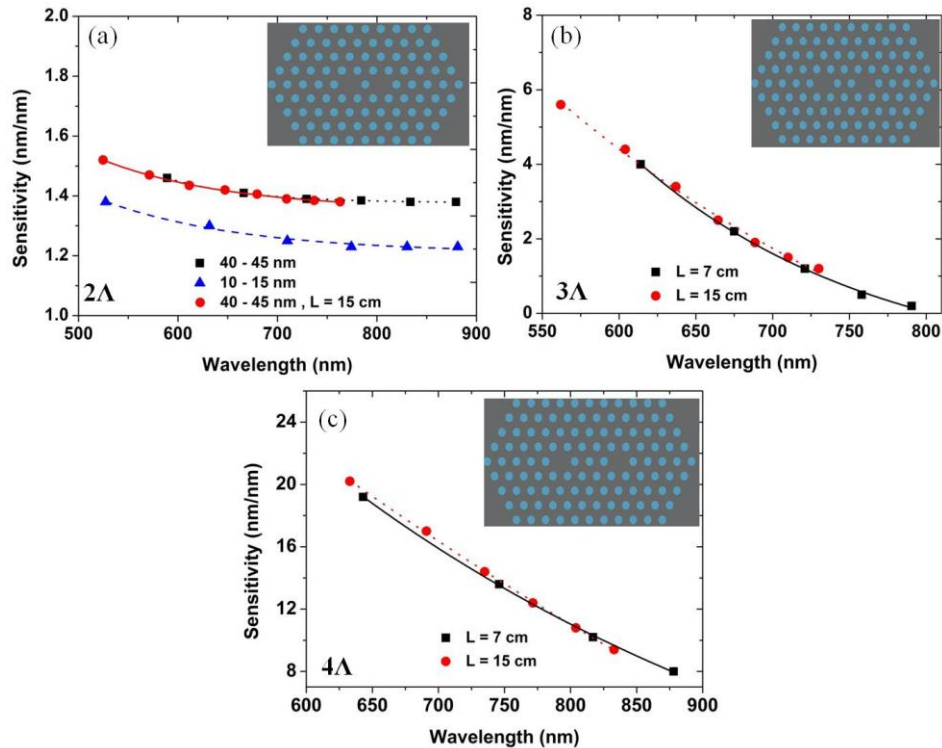

Fig. 6. Sensitivity versus wavelength of the dual-core mPOF biosensor for a separation of (a) 2Λ (comparison of 40-45 and 10-15 nm layer thickness for L = 7cm), (b) 3Λ and (c) 4Λ between the cores. Square dots correspond to a fiber length of L = 7 cm and red dots to L = 15 cm. The solid, dashed and dotted lines are the exponential fitting for each case.

In Fig. 6(b) we show the sensitivity of the dual-core mPOF with two holes (3Λ) between the cores. As expected the sensitivities for the two device lengths of 7 cm and 15 cm lie on the same curve, but the sensitivity is now higher. The maximum sensitivity is now 5.6 nm/nm at 560 nm and again the sensitivity decreases monotonically. However, the slope of the S(λ) curve is much steeper, as shown in Fig. 4(b), and thus there is much to be gained by operating at shorter wavelengths. Thus the maximum sensitivity for a 7 cm device is 4.0 nm/nm at 610 nm, while increasing the length to 15 cm allows to operate at a shorter wavelength of 560 nm and thereby increase the sensitivity to 5.6 nm/nm

By increasing the core separation to 3 holes (4Λ), Fig. 6(c) shows that the sensitivity reaches a level as high as 20 nm/nm at around 630 nm for the 15 cm long device. Importantly, this sensitivity is twice the hitherto record of 10.4 nm/nm using FWM [17].

4. Conclusion

We have proposed a dual-core mPOF suitable for label-free and selective biosensing. The evanescent wave sensing is carried out inside the holes of the mPOF, which makes the sensor robust, while the dual-core functionality means that no post processing of the fiber is required as e.g., when using grating-based sensors. The basic operation principle relies on tracking the shift of an extremum in the transmittance when the sensor captures a layer of antibody biomolecules.

In our design, we considered a PMMA mPOF with a hexagonal hole structure with a hole diameter of 1 μm and a pitch of Λ = 2 μm. We calculated the coupling lengths for three different dual-core mPOFs with 2Λ, 3Λ and 4Λ core separation and a fixed fiber length of 7 cm and 15 cm. All the design parameters of the dual-core mPOF design are feasible for fabrication and operation and no selective filling is required. In order to verify the appropriate length of the device, we experimentally measured the loss of a single-core mPOF with the same characteristics as the proposed dual-core coupler.

Our results demonstrate that the sensitivity increases with increasing the distance between the solid cores, as also observed by Town *et al.* for planar structures in a study of refractive index sensing [31]. The distance of course cannot be increased indefinitely, given that the structure has to fit into a preform of a realistic size below 80 mm, where we use 60 mm, and given that hole sizes less than 1.5 mm are impossible to drill sufficiently deep to obtain a long enough preform. A further limitation is in terms of loss, given that the necessary length of the fiber increases with increased core separation.

The sensitivities of the most sensitive dual-core mPOF with 4Λ distance between the cores is for example 20.3 nm/nm at the He-Ne wavelength 633 nm and 8.9 nm/nm at 850 nm, where cheap CMOS technology is available. At these two important wavelengths the loss of our fiber is around 0.15 dB/cm and 0.07 dB/cm, respectively. This is acceptable when considering device lengths less than 15 cm. We note that, the loss can be reduced further, as described in Section 2, to levels less than 1dB/m, as reported by Large *et al* [29].

Our record sensitivity of 20.3 nm/nm, i.e., a shift of the resonant peak of transmittance of 20.3 nm per nm thickness of biolayer, is therefore obtained for experimentally very feasible design parameters. The sensitivity is twice the hitherto predicted record of 10.4 nm/nm for a MOF-based biosensor, which required longer fiber lengths and a high-power laser [17].